

# Grain alignment in dense interstellar environments: Spectropolarimetry of the 4.67 $\mu$ m CO ice feature in the field star Elias 16 (Taurus Dark Cloud)

J. H. Hough<sup>1\*</sup>, D. K. Aitken<sup>1</sup>, D. C. B. Whittet<sup>2</sup>, A. J. Adamson<sup>3</sup>, and A. Chrysostomou<sup>1</sup>

<sup>1</sup> Centre for Astrophysics Research, Science & Technology Research Centre, University of Hertfordshire, AL6 0BE, UK

<sup>2</sup> Department of Physics and Astronomy, Rensselaer Polytechnic Institute, Troy, NY 12180-3590

<sup>3</sup> UK Infrared Telescope, Joint Astronomy Centre, 660 North A'Ohoku Place, Hilo, HI 96720

## ABSTRACT

We present spectropolarimetry of the solid CO feature at 4.67  $\mu$ m along the line of sight to Elias 16, a field star background to the Taurus Dark Cloud. A clear increase in polarization is observed across the feature with the peak of polarization shifted in wavelength relative to the peak of absorption. This shows that dust grains in dense, cold environments (temperatures  $\sim$ 20K or less) can align and produce polarization by dichroic absorption. For a grain model consisting of a core with a single mantle, the polarization feature is best modelled by a thick CO mantle, possibly including 10% water-ice, with the volume ratio of mantle to bare grain of  $\sim$ 5. Radiative torques could be responsible for the grain alignment provided the grain radius is at least 0.5  $\mu$ m. This would require the grain cores to have a radius of at least 0.3  $\mu$ m, much larger than grain sizes in the diffuse ISM. Sizes of this order seem reasonable on the basis of independent evidence for grain growth by coagulation, as well as mantle formation, inside dense clouds.

**Key words:** dust, extinction – infrared: ISM – ISM: lines and bands – ISM: magnetic fields – polarization – stars: individual (Elias 16).

## 1 INTRODUCTION

It has been long established that astrophysical dust grains can align in a variety of environments, but the mechanism(s) responsible are still not well understood. Developing a robust model of grain alignment is an important goal because magnetic fields play vital roles in astrophysical processes, on size scales from circumstellar disks to entire galaxies, and the polarization that results from grain alignment provides the means to study magnetic fields if the alignment process is fully understood. What seems clear is that alignment in diffuse regions of the interstellar medium (ISM) depends, in general, on an interaction between the magnetic properties of the grains and their rotational dynamics. The classical DG mechanism (Davis & Greenstein 1951), which assumes thermally spinning paramagnetic grains, correctly predicts the direction of alignment with respect to the Galactic magnetic field, but fails quantitatively to produce sufficient alignment to explain the observed amplitude of polarization. Enhancements to DG alignment have been

proposed that invoke grains with superparamagnetic properties, or with suprathermal spin resulting from molecule formation or radiative torques (see Lazarian 2003 and Roberge 2004 for recent reviews). However, a recent paper by Lazarian and Hoang (2007) shows that radiative torques can align grains without including paramagnetic relaxation.

Whilst early (optical) measurements of interstellar polarization were dominated by dust in diffuse (low optical depth) regions of the ISM, observations at infrared wavelengths over the past decade have provided data for much denser environments. It has been shown that the polarization efficiency, as measured by the ratio of linear polarization amplitude to optical depth ( $p/\tau$ ), declines with increasing extinction for stars that sample dust in dark clouds (Goodman et al. 1995; Gerakines et al. 1995; Arce et al. 1998; Whittet et al. 2001, 2007). It is inferred that grains within the clouds are generally less well aligned than those in the diffuse ISM, a result that is, indeed, consistent with all extant alignment mechanisms: resurfacing of grains with ice mantles thereby reducing the effectiveness of the Purcell mechanism (Purcell 1979), attenuation of the external radiation field, and closer coupling of dust and gas temperatures

\*E-mail: j.h.hough@herts.ac.uk

with increasing density all naturally lead to poorer alignment within dense clouds (Lazarian et al. 1997). It has been suggested that much of the observed polarization in the lines of sight toward stars in and behind dark clouds may arise in the diffuse outer layers of the clouds and not within them (e.g. Goodman et al. 1995).

However, other evidence shows unequivocally that grains do align in dense environments. Mid-infrared (Smith et al. 2000 and references therein), far-infrared and submillimetre observations of the polarized emission from dust indicate that the grains align with the local magnetic field in star forming regions (Hildebrand et al. 1999). Smith et al. (2000) show that in the mid-infrared  $p/\tau$  remains at roughly 1.5% for optical depths of the silicate feature ranging from 1 to 7 ( $A_V \sim 20$  to 120 mag.), and Vaillancourt (2002) shows that in some lines of sight the polarisation increases at wavelengths beyond  $350\mu\text{m}$ , implying alignment of a population of very cold grains deep within the clouds. Cho & Lazarian (2005) show that radiative torques, originally invoked in the 1970s (Dolginov 1972, Dolginov & Mytrophanov 1976), can be very efficient in producing alignment of large grains inside dense clouds, even for  $A_V \sim 10$  mag. It may thus be possible to account for the observed submm and mm polarizations in terms of polarized emission from large grains within the clouds.

Another excellent observational test of alignment within dense clouds is polarization associated with infrared absorption features produced by ice mantles on the grains. If excess polarization corresponding to an ice feature is detected then it follows that grains must be aligned to some degree in environments where the mantles can form, and this typically occurs in dark clouds and star formation regions with extinction  $A_V > 3$  mag for  $\text{H}_2\text{O}$ -dominated ices (e.g. Whittet et al. 2001). Polarization corresponding to the  $3.0\mu\text{m}$   $\text{H}_2\text{O}$ -ice feature has been observed in a number of lines of sight (e.g. Hough et al. 1988, 1989, 1996; Holloway et al. 2002). In principle, the CO ice feature at  $4.67\mu\text{m}$  provides an even more stringent test of grain alignment: in pure form, solid CO is expected to survive on the surfaces of grains only in the densest and coldest environments of molecular clouds ( $T < 20$  K), where the temperatures of the gas and grains must be close to thermodynamic equilibrium. Some CO may be trapped in  $\text{H}_2\text{O}$ -ice that can survive at higher temperature, but in most lines of sight the CO appears to be predominantly in a pure or nearly pure form (Tielens et al 1991; Chiar et al. 1995; Pontoppidan et al. 2003). Polarization associated with the  $4.67\mu\text{m}$  CO feature was first detected by Chrysostomou et al. (1996) in the line of sight

to W33A, an embedded YSO. Those observations suggest that grains must align within the dense molecular cloud. However, it has been argued that the embedded YSO itself may impose alignment of the grains, providing significant anisotropies in the radiation (Draine & Weingartner 1996; Onaka 2000) and/or velocity fields (Lazarian 1997).

A better means of testing grain alignment in dense clouds is via observations of background field stars unconnected with the clouds themselves. An excellent candidate is the well-studied field star Elias 16, a K2 giant background to the Taurus Dark Cloud (Elias 1978) with 24 magnitudes of visual extinction and deep ice features (Whittet et al. 1983, 1998, 2007; Chiar et al. 1995). The  $3.0\mu\text{m}$   $\text{H}_2\text{O}$ -ice feature is known to be polarized (Hough et al. 1988), indicating alignment of at least some of the ice-mantled grains in the line of sight. The CO ice absorption feature at  $4.67\mu\text{m}$  has an optical depth  $\tau \sim 1$  (Chiar et al. 1995). The profile is consistent with  $\sim 86\%$  of the CO being in a cold ( $T \sim 10$  K),  $\text{H}_2\text{O}$ -poor ice matrix, a fraction somewhat higher than is typical of embedded YSOs (e.g.  $\sim 74\%$  for W33A; Chiar et al. 1998). In the present paper, we report the first detection of polarization associated with the  $4.67\mu\text{m}$  feature in Elias 16.

## 2 OBSERVATIONS AND DATA REDUCTION

The data were obtained using the United Kingdom Infrared Telescope (UKIRT) on the nights of 15-16 February, 2006. UKIRT's facility imaging spectrograph, UIST, was used to obtain spectropolarimetry in the M band. The instrument optics include an internal Wollaston prism which is used as the polarimetric analyser, splitting the incoming radiation into the orthogonally polarized e- and o-beams which then pass through an M band grism. A focal plane mask, of length 20 arcsec, was used to avoid the overlap of e- and o-beams on the array. The source was nodded up and down the 5-pixel wide ( $0.6$  arcsec) slit following a standard ABBA sequence. The resolving power of the final spectrum was  $R \sim 800$ . BS1387 (A7IV-V star with  $V=4.2$ ) was used as a calibrator while the BN object in Orion KL was observed in order to check the position angle calibration, with its PA taken as 115 degrees (Johnson et al. 1981). The data were observed in the usual sequence of waveplate positions (0, 45, 22.5, 67.5 degrees) and those angles plus 90 degrees (i.e. 90, 135, 112.5 and 157.5 degrees) which avoids most of the ripple in the polarization and position angle spectra, produced by multiple reflections within the plates of the waveplate assembly (Aitken & Hough 2001). Unfortunately an equipment setup

error rendered the 112.5 and 157.5 degree positions incorrect, and meant that although a ripple-free Q spectrum was available, the corresponding U spectrum was not. Data reduction therefore proceeded using only the first four position angles. The raw data frames were dark subtracted, flat-fielded and sky subtracted in the usual manner. Wavelength calibration was achieved by fitting to the OH lines in the spectrum, using wavelengths from the M band OH line list compiled for the SpeX instrument on the IRTF. The e- and o-beam spectra were extracted and the Stokes parameters obtained using the usual RATIO method, for the Stokes Q parameter with data taken at 0 and 45 degrees:  $R_Q^2 = (I_e/I_o)/(I_e/I_o)_{45}$  and  $q = Q/I = (R_Q - 1)/(R_Q + 1)$ . The Stokes U parameter is determined in the same manner using exposures taken at the 22.5 and 67.5 degree waveplate positions. The polarisation and position angles are then calculated in the usual manner,  $p = (u^2 + q^2)^{1/2}$  and  $\vartheta = 0.5 \tan^{-1}(u/q)$ . Ripples in the Q and U spectra Stokes were removed using a Fourier filter (see Adamson et al. 1999).

### 3 RESULTS AND DISCUSSION

#### 3.1 Continuum fit and optical depth profile

Intensity was converted to optical depth by fitting a linear continuum to the spectrum in regions adjacent to the CO feature (4.60 – 4.65 and 4.71 – 4.85  $\mu\text{m}$ ), as shown in Fig. 1. The profile of the CO feature is consistent with previous observations that suggest the presence of superposed broad and narrow components (Tielens et al. 1991; Chiar et al. 1995; Pontoppidan et al. 2003). A fit to the profile was made using the 3-component empirical formulation proposed by Pontoppidan et al. (2003), illustrated in Fig. 2. The profile is dominated by the middle component, which Pontoppidan et al. attribute to essentially pure CO ice, accounting for ~ 88% of the optical depth at the peak of the feature. These results corroborate the results of the earlier study by Chiar et al. (1995): most of the solid CO toward Elias 16 resides in a CO-rich (and H<sub>2</sub>O-poor) phase of the ice mantles in the line of sight.

#### 3.2 The polarization feature

Fig 3(a) shows the observed polarization spectrum for Elias 16, and Fig 3(b) shows a comparison of the observed optical depth and polarization profiles, with the continuum polarization of 0.56% subtracted. There is a shift to the red in the position of the polarization feature relative to the optical depth feature, as expected for dichroic extinction by aligned

grains: the absorption coefficients of non-spherical grains are different for E-vectors vibrating perpendicular and parallel to the axis of symmetry, shifting the polarization peak to longer wavelength relative to extinction at a resonance (Kobayashi et al. 1980; Aitken 1989). This provides clear observational evidence that grains in dense cold regions do align. The magnitude of the observed shift in Elias 16 is  $(0.0034 \pm 0.0005) \mu\text{m}$ , comparable with that previously seen for the CO feature in W33A ( $0.004 \pm 0.001 \mu\text{m}$ ; Chrysostomou et al. 1996). The shift for the 3 $\mu\text{m}$  water-ice feature is much larger, with a value of ~0.05  $\mu\text{m}$  for the BN object (Hough et al. 1996), consistent with the 20 times higher band strength for water-ice compared to CO-ice (Gerakines et al. 1995).

The ratio of polarization to optical depth ( $p/\tau$ ) in the feature, also known as the specific polarization, is a measure of the efficiency of polarization production by grains along the line of sight. For the CO ice feature in Elias 16 the peak of polarization is  $(1.20 \pm 0.10)\%$  and the peak optical depth is  $(1.05 \pm 0.02)$ , giving a  $p/\tau$  ratio of  $(1.14 \pm 0.10)\%$ , which is comparable to that observed in W33A (~1.0%; Chrysostomou et al. 1996). The corresponding ratio in the H<sub>2</sub>O ice feature in Elias 16 is  $(0.9 \pm 0.15)\%$  (Hough et al. 1988), and that in the K-band continuum is ~ 1.24% (Whittet et al. 2007 and references therein). It is surprising that the CO feature is as efficiently polarized as the H<sub>2</sub>O feature in Elias 16, as the CO-ice is formed in colder denser regions.

The position angle (not shown) of the continuum polarization is  $(73 \pm 2.3)$  degrees, increasing in the CO feature to  $(86 \pm 4.2)$  degrees. This compares with a continuum polarization of  $(73 \pm 1.5)$  degrees in the 3  $\mu\text{m}$  band and  $(76 \pm 1.4)$  degrees in the 3 $\mu\text{m}$  water-ice feature. All these position angles are weighted means and that they are different shows the fractionation of material. If the field direction twists fairly steadily along the line of sight then an increasing progression in PA from bare grains with PA 73 degrees, to water ice-mantled grains with PA 76 degrees, to CO-mantled grains with PA 86 degrees, would be expected, with the changes in PA depending on the degree of twist. The different position angles will give rise to circular polarization, which should also show the features in a manner which would then indicate their relative distances along the line of sight (Aitken, Hough & Chrysostomou, 2006).

### 4 MODELLING

In general, ices form on existing structures and since we are concerned with producing

polarization with the spectral characteristics of solid CO, silicate grains as mantle cores offer a particular attraction. They are known to be aligned by magnetic fields and do retain this property when supporting mantles of, for instance, H<sub>2</sub>O ice since its polarized feature has often been observed (Hough et al. 1988, 1989, 1996; Holloway et al. 2002). Nevertheless, an interface between materials of different optical properties, such as occurs in a core/mantle system, can become the site of induced charges which alter the electric field within the grain from that expected from their bulk optical properties, and this is especially true for small and non-spherical or irregular structures. For solid CO, whose dielectric function,  $\varepsilon = \varepsilon' + i\varepsilon''$  is a strong function of wavelength in which the real part,  $\varepsilon'$ , goes negative between 4.663 and 4.676 $\mu\text{m}$  the effects can be very noticeable. Particularly good treatments of this behaviour are given in Tielens et al. (1991), with reference to solid CO, and also in Huffman (1977).

For analytical shapes capable of producing polarization we have used spheroids, the simplest shapes beyond spheres, having just two axes of equal length. Spheroids are ellipses rotated about either a major or minor axis, producing respectively prolate or oblate spheroids. Oblate spheroids have been used here, partly because there is some evidence that they produce a better match to observed silicate polarizations (Hildebrand 1988), and for a given degree of alignment there is a factor two more polarization from them than from prolate shapes. Grain cross sections are determined in the Rayleigh limit with  $C_{\parallel}$  the value viewed along the symmetry axis and  $C_{\perp}$  viewed normal to it. For a mantle of solid CO, the dielectric function is taken from Hudgins et al. (1993), or from Tielens et al. (1991) for contaminated CO, and for the core silicate the astronomical silicate of Draine (1985) is used. The cross section algorithms used are taken from Draine and Lee (1984) for both bare and mantled grains in which the mantle outer surface is assumed confocal with that of the core.

In general it has been found that relatively mild eccentricities are needed to produce adequate polarizations, and this also seems to be true in the present case. We have taken a silicate core with eccentricity  $b/a=1.25$ , and a confocal mantle of CO with outer surface  $b/a=1.24$ , which determines a mantle/core volume ratio,  $M/C$ , of 0.09. Fig 4(a) shows, for these grains,  $(2C_{\perp} + C_{\parallel})/3$ , which is an estimate of extinction from an assembly of unaligned grains, and  $C_{\perp}-C_{\parallel}$ , the polarization fraction expected for an assembly of completely aligned grains with their grain symmetry axes confined to the plane of the sky, plotted against wavelength. The extinction

profile shows a marked double-peak (see also Tielens et al. 1991) that is not observed in the CO feature of any published data, but the completely aligned polarization, at the same wavelength as the second peak, could be as much as 30% , so the mild eccentricity seems adequate.

The structure in the extinction profile can be reduced by introducing impurities into the CO mantle or by increasing the mantle thickness. The second effect is shown in Fig 4(b) which is for the same silicate core but where the CO mantle is confocally grown further until the outer surface has  $b/a=1.1$ ,  $M/C$  becomes 4.66, and the grain size is increased by a factor around 1.7. Fewer grains will now produce the required extinction and the polarization is still adequate, although some structure in the extinction profile is still observed. Fig 4(c) shows the effect of also including some H<sub>2</sub>O ice in the mantle. Here the dielectric function is from Table 4 in Tielens et al. (1991) and the CO/H<sub>2</sub>O ratio is 10/1. The same silicate core eccentricity is used, the same (impure) mantle grown confocally to  $b/a=1.1$ , with  $M/C=4.66$ . Except for the slight elevation of extinction around 4.65 to 4.66 $\mu\text{m}$  this model is a reasonable fit to the data (Fig 5), with the double-peaked structure now suppressed, and with a similar small shift between the extinction peak and polarization peak to that observed (see section 3.2). The completely aligned polarization would be 17% and the negative, or 180° shifted component, would steepen the short wave profile, as seems to be observed.

These model fits, with large CO mantles, are dominated by the CO and produce little continuum extinction or polarization, whereas continuum polarization is observed at the half percent level. With such a mantle, the continuum must come from other and bare grains, possibly from a different part of the line of sight.

We conclude that reasonable fits to the observed data require volume ratios of CO mantle to silicate core of  $\sim 5$ , with much smaller ratios producing marked double peaked extinction profiles. Of order 10% water-ice needs to be added to the CO mantle so as to totally suppress the double-peaked feature. Interestingly, bare CO without a core produces reasonable fits (not shown), although the polarization reversal is rather deep, and presumably a silicate core is needed in order to act as a seed for the formation of ices and to enable the grains to align. High volumes of mantle to core is consistent with the modelling of the water ice feature along the line of sight to the BN protostar with a ratio between 0.5 and 5.0, with the upper limit set by abundance constraints (Lee & Draine 1985). High mantle to core volumes for solid CO are also possible although it does depend on the amount of CO that freezes

onto the grains. Smith, Sellgren & Brooke (1993), fitting to the extinction profiles for the water-ice feature in Taurus, and employing a model consisting of ice-mantled graphite and silicate cores, find that either the grains have a variable mantle thickness, with most of the ice on the larger grains, or there are two grain populations in Taurus, one comprising bare grains and the other comprising grains with  $0.35\mu\text{m}$  thick ice-mantles, in a ratio  $3\times 10^4:1$ . In either case, the mantled grains are much larger than the bare grains.

In practice the CO-ices will be deposited on grains that already have substantial water-ice mantles, leading to even larger grain sizes (see next section). The modelling of grains with two confocal mantles is beyond the scope of this paper.

## 5 IMPLICATIONS FOR GRAIN ALIGNMENT

Spectropolarimetry of the solid CO feature shows that grains carrying the feature are aligned, with a clear enhancement of polarization across the feature and with the peak of polarization slightly redward of the peak of absorption, an important diagnostic of polarization produced by dichroic absorption. As noted in section 3.2, the efficiency of grain alignment, as measured by  $p/\tau$ , is comparable to that observed in the CO feature along the line of sight to W33A, and to the corresponding ratio in the  $\text{H}_2\text{O}$  ice feature in Elias 16, and that in the K-band continuum. Thus, not only do the carriers of the CO feature align but the efficiency of alignment does not appear to be reduced in the dense cold regions where CO mantles form and does not require the presence of an embedded source to provide the radiation source (as may occur in the case of W33A).

Cho & Lazarian (2005) show (their Figure 2) that radiative torques can produce suprathermal rotation even for large  $A_v$ , provided the grains are large. As noted by these authors, other mechanisms that produce suprathermal rotation are also more effective for large grains as they are not as sensitive to the cancellation of the resulting torques by grain flipping and becoming thermally trapped. However, spin-up processes such as the formation of  $\text{H}_2$  on grain surfaces, and subsequent ejection from preferential sites (Purcell, 1979), will not occur in the dense regions of clouds where little atomic hydrogen will exist. Cho & Lazarian show that a GMC located 5kpc from the Galactic centre, with an  $A_v$  of 10 mag., requires grain sizes larger than about  $0.2\mu\text{m}$ , with the efficiency of radiative torques increasing strongly with increasing grain size. Elias 16 has an extinction  $A_v \sim 20\text{-}25$ , but as the

star lies behind the Taurus cloud,  $A_v \sim 10$  is a reasonable representation of the attenuation of the external interstellar radiation field within the cloud, averaged along the line of sight. Figure 3 of Cho & Lazarian shows that the minimum grain size for alignment is a very strong function of the cloud density. For the Taurus Dark Cloud, gas densities vary from  $10^2 \text{ cm}^{-3}$  in regions of low density (Sakamoto & Sunada 2003) to  $10^4 - 10^5 \text{ cm}^{-3}$  in the densest cores (Gaida et al. 1984). For an  $A_v$  of 10 mag. and a density of  $10^4 \text{ cm}^{-3}$ , the minimum grain size for effective alignment is  $0.4\mu\text{m}$ , and  $0.6\mu\text{m}$  for a density of  $10^5 \text{ cm}^{-3}$ . Although this is much larger than the  $0.25\mu\text{m}$  cut-off for the diffuse ISM (Mathis et al. 1977), Cho & Lazarian (and references therein) point out that larger grains are expected to be abundant in dark clouds, formed through coagulation. Bowey, Adamson & Whittet (1998), from a comparison of the  $10 \mu\text{m}$  profiles of molecular cloud and diffuse ISM silicate dust, suggest possible grain growth in the denser environment along the line of sight to Elias 16. Whittet et al. (2001) provide observational evidence for an increase in  $R_v$  for the Taurus Dark Cloud, from 3.0 to 4.5 from the diffuse screen to within the dense clumps, and the mean grain radius scales with  $R_v$  if the refractive index is unchanged, which would be the case for coagulation. Grain growth has also been invoked to explain saturation of the relationship between  $A_v$  and silicate optical depth in dark clouds at  $A_v \sim 10$  mag. (Chiar et al. 2007). Also, our model calculations of section 4 suggest that the volume of mantle to core is 4.0-5.0, giving an increase in grain size of  $\sim 70\text{-}80\%$  compared to bare grains, and the models of Smith, Sellgren & Brooke (1993) indicate a  $\sim 0.35\mu\text{m}$  thick water-ice mantle on grains in Taurus. Thus, ice-mantled grains, being significantly larger, will normally be better aligned. If, as expected, the CO-ices are formed on water-ices then the grain sizes will be even larger. For example, similar volume ratios of water-ices and CO-ices, to the grain core, will increase the grain radius by over a factor of 2. This will reduce the requirement for significant grain growth in order for radiative torques to align the grains, or if grain growth is substantial then this would lead to even higher efficiency in the alignment of those grains with both water and CO ice mantles. A more extensive study of grain alignment in dense interstellar clouds is given in Whittet et al (2007), including a comparison with the recent radiative torque model of Lazarian and Hoang (2007).

## 6 CONCLUSIONS

We have shown that CO-mantled grains along the line of sight to the star Elias 16, background

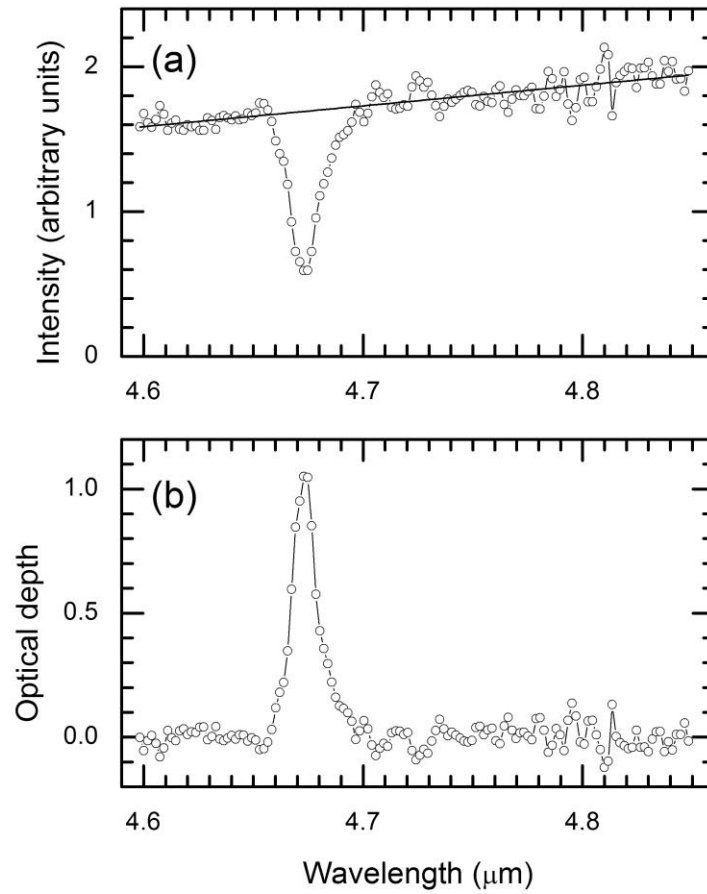
to the Taurus Dark Cloud, are at least as efficiently aligned as grains with water-ice mantles and bare grains. This is despite CO-mantled grains only existing in dense environments with temperatures  $\sim 20\text{K}$  or less. Modelling of the extinction and polarization profiles requires large CO mantles, with mantle to silicate core volumes of at least  $\sim 5$ , and with a  $\sim 10\%$  impurity, such as water-ice, in order to suppress any double-peaked features that do not occur in the observational data. This growth in grain size would aid alignment through radiative torques.

**ACKNOWLEDGMENTS** We would like to thank John Rayner for providing the calibration wavelengths of the OH lines. The United Kingdom Infrared Telescope is operated by the Joint Astronomy Centre on behalf of the Science and Technology Facilities Council of the UK.

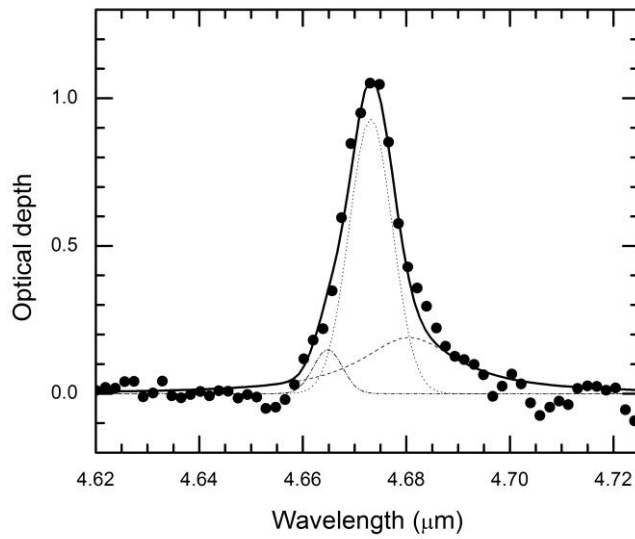
## REFERENCES

- Adamson A. J., Whittet D. C. B., Chrysostomou A., Hough J. H., Aitken D. K., Wright G. S., Roche P. F., 1999, *ApJ*, 512, 224
- Aitken D. K. 1989, in *Infrared Spectroscopy in Astronomy*, Proceedings of the 22nd Eslab Symposium, ed. by B.H. Kaldeich. p99
- Aitken D. K., Hough J. H., 2001, *PASP*, 113, 1300
- Aitken D. K., Hough J. H., Chrysostomou A., 2006, *MNRAS*, 366, 491
- Arce H. G., Goodman A. A., Bastien P., Manset N., Sumner M., 1998, *ApJ*, 499, 93
- Bowey J. E., Adamson A. J., Whittet D. C. B., 1998, *MNRAS*, 298, 131
- Chiar J. E., Adamson A. J., Kerr T. H., Whittet D. C. B. 1995, *ApJ*, 455, 234
- Chiar J. E., Gerakines P. A., Whittet D. C. B., Pendelton Y. J., Tielens A. G. G. M., Adamson A. J., Boogert A. C. A., 1998, *ApJ*, 498, 716
- Chiar J. E., Gerakines P. A., Whittet D. C. B., Pendelton Y. J., Tielens A. G. G. M., Adamson A. J., Boogert A. C. A., 1998, *ApJ*, 498, 716
- Chiar J. E., Ennico, K., Pendelton, Y. J., Boogert, A. C. A., Greene, T., Knez, C., Lada, C., Roellig, T., Tielens, A. G. G. M., Werner, M., Whittet, D. C. B., 2007, *ApJ*, 666, L73
- Cho J., Lazarian A., 2005, *ApJ*, 631, 361
- Chrysostomou A., Hough J. H., Whittet D. C. B., Aitken D. K., Roche P. F., Lazarian A., 1996, *ApJ*, 456, L61
- Davis L., Greenstein J. L., 1951, *ApJ*, 114, 206
- Dolginov A. Z. 1972, *Ap&SS*, 18, 337
- Dolginov A. Z., Mytrophanov, I. G., 1976, *Ap&SS*, 43, 291
- Draine B. T., 1985 *ApJS*, 57 587
- Draine B., Lee, H., 1984, *ApJ* 285, 89
- Draine B. T., Weingartner J., 1996, *ApJ*, 470, 551
- Elias J. H., 1978, *ApJ*, 224, 857
- Gaida M., Ungerechts H., Winnewisser G., 1984, *A&A*, 137, 17
- Gerakines P. A., Whittet D. C. B., Lazarian A., 1995, *ApJ*, 455, L171
- Gerakines P. A., Schutte W. A., Greenberg J. M., van Dishoeck E. F., 1995, *A&A*, 296, 810
- Goodman A. A., Jones T. J., Lada E. A., Myers P. C., 1995, *ApJ*, 448, 748
- Hildebrand R. H., 1988, *J. Quant. Spectr. Rad. Trans.*, 29, 3, 327
- Hildebrand R. H., Dotson J. L., Dowell C. D., Schleuning D. A., Vaillancourt J. E., 1999, *ApJ*, 516, 834
- Holloway R. P., Chrysostomou A., Aitken D. K., Hough J. H., McCall A., 2002, *MNRAS*, 336, 425
- Hough J. H., Sato S., Tamura M., Yamashita T., McFaddean A. D., Rouse, M. F. Whittet D. C. B., Kaifu N., Suzuki H., Nagata T., Gatley I., Bailey J., 1988, *MNRAS*, 230, 107
- Hough J. H., Whittet D. C. B., Sato S., Yamashita T., Tamura M., Nagata T., Aitken, D. K., Roche, P. F., 1989, *MNRAS*, 241, 71
- Hough J. H., Chrysostomou A., Messinger D. W., Whittet D. C. B., Aitken D. K., Roche P. F., 1996, *ApJ*, 461, 902
- Hudgins D. M., Sandford S. A., Allamandola L. J., Tielens A. G. G. M., 1993, *ApJS*, 86 713
- Huffman D. R., 1977, *Advances in Physics*, 26, 129
- Johnson P. E., Rieke G. H., Lebofsky M. J., Kemp J. C., 1981, *ApJ*, 245
- Kobayashi Y., Kawara K., Sato S., Okuda, H., 1980, *PASJ*, 32, 295
- Lazarian A., 1997, *ApJ*, 483, 296
- Lazarian A., Goodman A. A., Myers P. C., 1997, *ApJ*, 490, 273
- Lazarian A., Hoang, T., 2007, *MNRAS*, 378, 910
- Lazarian A., 2003, *J. Quant. Spectr. Rad. Trans.*, 79-80, 881
- Lee H. M., Draine, B. T., 1985, 290, 211
- Mathis J., Rumpl W., Nordsieck K., 1977, *ApJ*, 217, 425
- Onaka T., 2000, *ApJ*, 533, 298
- Pontoppidan K. M., Dartois E., van Dishoeck E. F., Thi W.-F., d'Hendecourt L. 2003, *A&A*, 404, 17
- Purcell E. M., 1979, *ApJ*, 231, 404
- Roberge W.G., 2004, in *Astrophysics of Dust*, ASP Conference Series, 309, 467
- Sakamoto, S., & Sunada, K. 2003, *ApJ*, 594, 340
- Smith R. G., Sellgren K., Brooke T. Y., 1993, *MNRAS*, 263, 749
- Smith C. H., Wright C. M., Aitken D. K., Roche P. F., Hough J. H., 2000, *MNRAS*, 312, 327
- Tielens A. G. G. M., Tokunaga A. T., Geballe T. R., Bass, F., 1991, *ApJ*, 381, 181

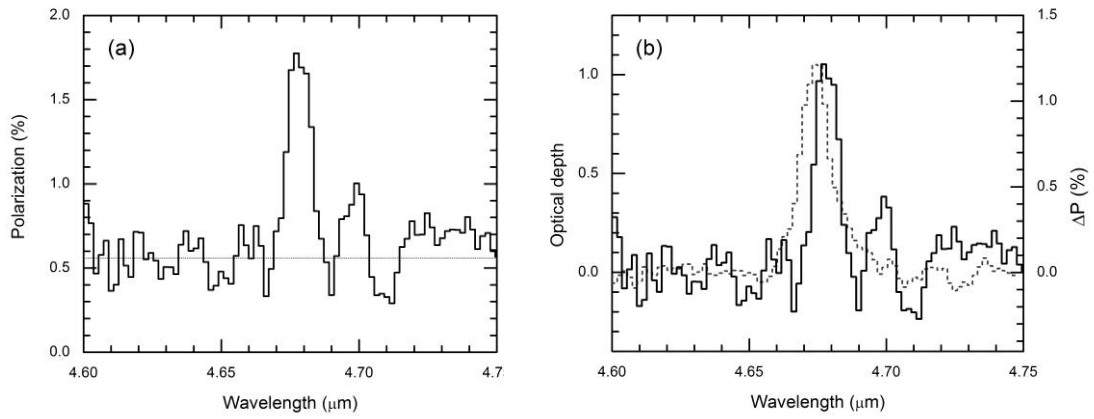
- Vaillancourt J. E., 2002, ApJS, 142, 53
- Whittet D. C. B., Bode M. F., Baines D. W. T.,  
Longmore A. J., Evans A., 1983, Nature, 303,  
218
- Whittet D. C. B., Gerakines P. A., Tielens A. G.  
G. M., Adamson A. J., Boogert A. C. A., Chiar  
J. E., de Graauw Th., Ehrenfreund P., Prusti T.,  
Schutte W. A., Vandenbussche B., van  
Dishoek E. F., 1998, ApJ, 498, L159
- Whittet D. C. B., Gerakines P. A., Hough J. H.,  
Shenoy S. S., 2001, ApJ, 547, 872
- Whittet D. C. B., Hough J. H., Lazarian, A.,  
2007, arXiv e-print (arXiv:0711.2536)



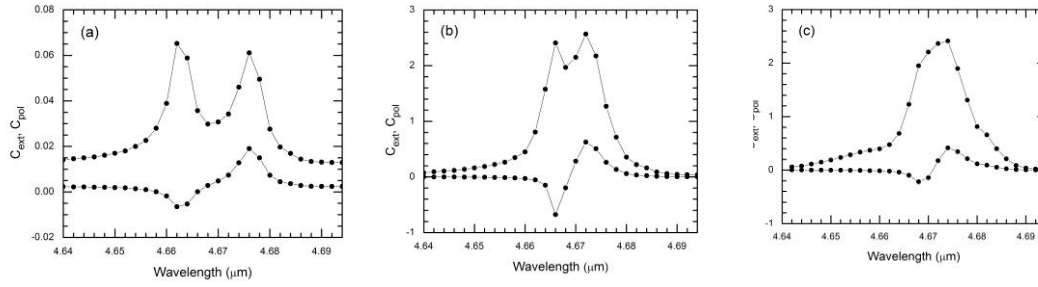
**Figure 1:** (a) Intensity spectrum, showing the adopted linear continuum, and (b) the resulting optical depth spectrum.



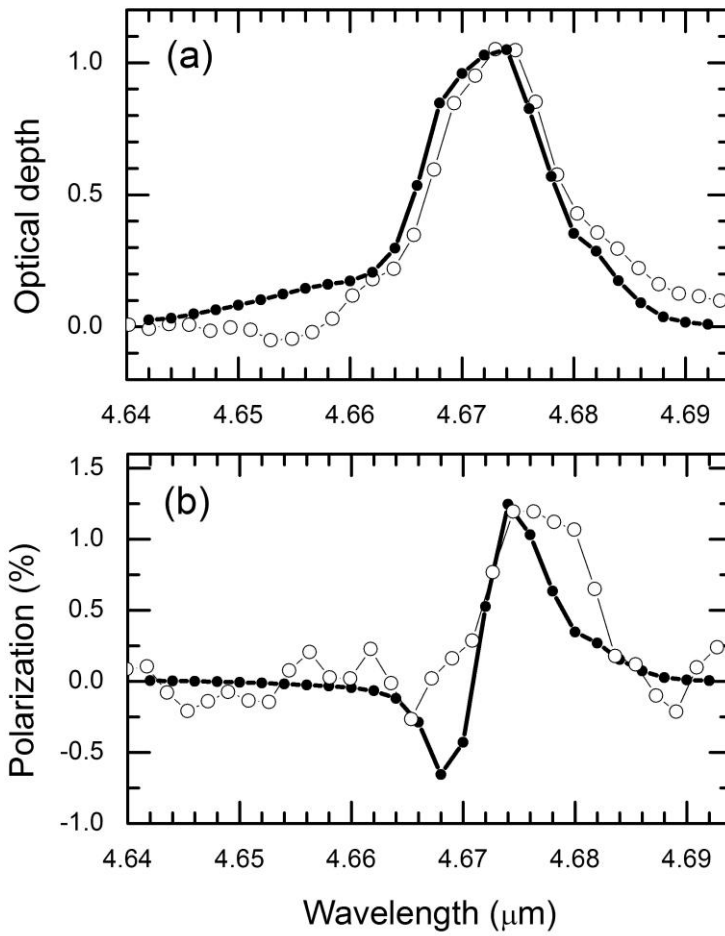
**Figure 2:** Three-component fit to the observed optical depth profile in Elias 16, based on the formulation of Pontoppidan et al. (2003). The components of the fit are, from left to right, (i) “blue” (dot-dash curve, Gaussian, centred at  $4.6648 \mu\text{m}$  ( $2143.7 \text{ cm}^{-1}$ ),  $\text{FWHM} = 3.0 \text{ cm}^{-1}$ , amplitude = 0.15), (ii) “middle” (dotted curve, Gaussian, centred at  $4.6749 \mu\text{m}$  ( $2139.1 \text{ cm}^{-1}$ ),  $\text{FWHM} = 4.5 \text{ cm}^{-1}$ , amplitude = 0.93), and (iii) “red” (dashed curve, Lorentzian, centred at  $4.6806 \mu\text{m}$  ( $2136.5 \text{ cm}^{-1}$ ),  $\text{FWHM} = 10.6 \text{ cm}^{-1}$ , amplitude = 0.19). The thick solid line is the sum of the three components. The peak optical depth at the centre of the feature is  $1.05 \pm 0.02$ .



**Figure 3:** (a) Polarization data (horizontal line shows the continuum polarization of 0.56%); (b) Comparison of optical depth (thin line, left-hand scale) and polarization, with the continuum removed, (thick line, right-hand scale), for the solid CO feature observed in Elias 16.



**Figures 4:** Model extinctions (upper curves) and polarizations (lower curves) using a silicate core with eccentricity,  $b/a=1.25$ , and a confocal mantle of CO; **(a):** with the outer surface  $b/a=1.24$  and a mantle/core volume ratio of 0.09; **(b):** The CO mantle is grown further until the outer surface has  $b/a=1.1$ , and the mantle/core volume ratio becomes 4.66, and the grain size is increased by a factor around 1.7; **(c):** 10% water-ice has been added to the CO and the impure mantle grown to  $b/a = 1.1$ , resulting in a value 4.66 for  $M/C$  (see the text for further details).



**Figures 5:** Comparison of observations (open circles) and models from Figure 4(c) (closed circles); **(a)** optical depth; **(b)** polarization, with the continuum polarization of  $\sim 0.5\%$  subtracted.